# Reversible Photobleaching of Enhanced Green Fluorescent Proteins†

Daniel Sinnecker, Philipp Voigt, Nicole Hellwig, and Michael Schaefer*

*Institut für Pharmakologie, Charité—Universitätsmedizin Berlin, Campus Benjamin Franklin, Thielallee 67-73, 14195 Berlin, Germany*

*Received September 30, 2004; Revised Manuscript Received January 29, 2005*

ABSTRACT: Color variants of green fluorescent protein (GFP) are increasingly used for multicolor imaging, fluorescence resonance energy transfer (FRET), and fluorescence recovery after photobleaching (FRAP). Here we show that experimental settings commonly used in these imaging experiments may induce an as yet uncharacterized reversible photobleaching of fluorescent proteins, which is more pronounced at acidic pH. Whereas the reversible photobleaching spectrum of eCFP corresponds to its absorption spectrum, reversible photobleaching spectra of yellow variants resemble absorption spectra of their protonated states. Fluorescence intensities recover spontaneously with time constants of 25−58 s. The recovery of eCFP can be further accelerated by illumination. The resulting steady-state fluorescence reflects a variable equilibrium between reversible photobleaching, spontaneous recovery, and light-induced recovery. These processes can cause significant artifacts in commonly applied imaging techniques, photobleach-based FRET determinations, and FRAP assays.

Green fluorescent protein (GFP) from *Aequorea victoria* and its color variants can be fused to other proteins by cloning techniques and develop fluorescence without additional cellular cofactors. GFP variants have, therefore, been extensively used to study the subcellular localization and trafficking of proteins in living cells. In addition, protein−protein interactions and intramolecular conformational changes can be followed by fluorescence resonance energy transfer (FRET[1]) between different color variants (*1*, *2*). For multicolor imaging experiments, fluorochromes should ideally exhibit stable fluorescence intensities, simple photobleaching kinetics, and invariable spectral properties. In particular, these preconditions are important for FRET experiments or for determination of fluorescence recovery after photobleaching (FRAP).

Wild-type GFP exhibits a complex photochromism, thus impairing its use in such experimental settings (*1*, *3*, *4*). To allow multicolor imaging and FRET experiments, efforts have been made to develop GFP mutants with simple photophysics and altered excitation/emission spectra. The replacement of Ser65 with Thr yielded red-shifted GFP variants (e.g. eGFP) with a stabilized absorption at 489 nm (*3*, *5*). Cyan fluorescent proteins (e.g. eCFP) have been developed (Tyr66 to Trp) and are currently the most frequently utilized FRET donor fluorochromes. Yellow fluorescent proteins, generated by the replacement of Thr203 with Tyr, are characterized by a marked sensitivity to protonation and halide binding (*1*, *6*). Citrine, a yellow variant containing a replacement of Gln69 with Met, has been reported to be superior to eYFP in terms of a lower p$K_a$, eliminated halide sensitivity, and improved folding at 37 °C (*6*). In FRET experiments applying *Aequorea*-GFP-related fluorescent proteins, yellow fluorescent proteins are typically used as FRET acceptors.

Although engineered GFP variants lack the pronounced photochromism of wild-type GFP (*1*), biophysical techniques such as single-molecule detection (*7*−*9*), spectral hole burning (*10*, *11*), and fluorescence correlation spectroscopy (*12*) have provided evidence that these variants do also exhibit photoconversion as well as single-molecule flickering at different time scales. The impact of this behavior on cell biological experiments has not yet been investigated.

Therefore, we characterized the photophysical properties of GFP variants and their relevance for fluorescence imaging applications in living cells. The frequently used eCFP, eGFP, eYFP, and Citrine are all susceptible to reversible photobleaching. This light-induced and pH-dependent phenomenon leads to the generation of a nonfluorescent species which recovers spontaneously or through illumination. These processes may cause significant artifacts in a number of commonly applied imaging techniques, including photobleaching-based FRET determinations and FRAP assays.

## EXPERIMENTAL PROCEDURES

*Construction of Expression Plasmids.* To generate eCFP-eYFP, the open reading frame of eYFP lacking the start codon was excised from pcDNA3-eYFP (*13*) and subcloned into the *Eco*RI and *Apa*I sites of pECFP-C1 (Clontech, Palo Alto, CA). The open reading frame of Citrine was amplified by PCR from YC3.3-pcDNA3 (6) and subcloned into the *Apa*I and *Xba*I sites of pcDNA3.1. eCFP-Citrine was generated by in-frame ligation of Citrine into the *Eco*RI and *Apa*I sites of pECFP-C1. For expression in *Escherichia coli*,

† This work was supported by the Deutsche Forschungsgemeinschaft and the Fonds der Chemischen Industrie.

* Corresponding author. Phone: +49-30-84451863. Fax: +49-30-84451818. E-mail: schae@zedat.fu-berlin.de.

[1] Abbreviations: eCFP, eGFP, eYFP, enhanced cyan, green, and yellow variants of green fluorescent protein; FRAP, fluorescence recovery after photobleaching; FRET, fluorescence resonance energy transfer.

10.1021/bi047881x CCC: $30.25 
Published on Web 04/14/2005

the coding sequences of the respective GFP variants were amplified by PCR, introducing a *Nco*I site and a sequence encoding a hexa-His tag at the 5' end and subcloned into pQE60 (Qiagen, Valencia, CA). All constructs were confirmed by cDNA sequencing (ABI-Prism 377; Perkin-Elmer, Norwalk, CT).

*Cell Culture and Transfection.* HEK 293 cells (ATCC, Manassas, VA) were grown at 37 °C under 5% $CO_2$ in minimal essential medium supplemented with Earle's salts, 10% FCS, 100 $\mu$g/mL streptomycin, and 100 units/mL penicillin. Cells were transiently transfected with plasmids encoding the respective proteins using the Fugene 6 transfection reagent (Roche Molecular Biochemicals, Mannheim, Germany).

*Bacterial Expression, Purification, and Absorption Spectroscopy of Fluorescent Proteins.* GFP color variants expressed in *E. coli* were purified by affinity chromatography using Ni-NTA resin (Qiagen). His-tagged proteins were eluted with elution buffer containing 20 mM Tris/HCl (pH 8), 20 mM NaCl, and 200 mM imidazole and subsequently subjected to ion exchange chromatography (Äkta purifier equipped with a Resource Q anion exchange column, Amersham Pharmacia, Piscataway, NJ). Proteins were eluted by applying a linear gradient of $Na_2SO_4$ (0 to 500 mM) in 20 mM Tris/HCl (pH 8). Fractions were analyzed by SDS−PAGE and Coomassie staining. Fractions containing apparently homogeneous fluorescent protein were used for the assays. Absorption spectra were recorded with a Cary 1E spectrophotometer (Varian, Walnut Creek, CA) in PBS supplemented with 10 mM sodium acetate and 12.5 mM imidazole, adjusted to the respective pH with phosphoric acid.

*Fluorescence Imaging.* Imaging experiments were performed at room temperature in HEPES-buffered saline (HBS), containing 138 mM NaCl, 6 mM KCl, 1 mM $MgCl_2$, 1 mM $CaCl_2$, 5.5 mM glucose, 10 mM HEPES (pH 7.4), and 0.2% (w/v) BSA. To change the intracellular pH ($pH_i$), cells were equilibrated in a $K^+$-based HBS (128 mM KCl and 10 mM NaCl) adjusted to the indicated pH and supplemented with 10 $\mu$M nigericine. Coverslips were mounted onto the stage of an inverted epifluorescence microscope (Axiovert 100, Carl Zeiss, Göttingen, Germany) with a 63×/1.4 Plan-Apochromat or a 40×/1.3 F-Fluar objective (both Carl Zeiss). Monochromic light was obtained with a xenon lamp and a computer-controlled fast switching monochromator (Polychrome IV, TILL-Photonics, Martinsried, Germany) and directed to the sample through an 80/20 semireflective mirror (Chroma Technology, Brattleboro, VT). Band-pass emission filters (Chroma) changed by a motorized filter wheel (Lambda 10/2; Sutter Instruments, Novato, CA) were used for separate detection of eYFP or Citrine (540−580 nm) and eCFP (460−500 nm). Fluorescence was detected with a cooled 12-bit CCD camera (IMAGO, TILL-Photonics). Unless otherwise stated, exposure times equal the actual illumination times of the sample. Fluorescence intensities were recorded over multiple single cells and corrected for background signals, determined over untransfected cells in the same visual field.

## RESULTS

*Reversible Photobleaching of GFP Color Variants.* In fluorescence imaging experiments using eCFP-expressing cells, we consistently observed a decrease in the eCFP fluorescence at the beginning of the experiment (Figure 1a). This effect was evident at physiological pH, but even more obvious at acidic intracellular pH (Figure 1b). These experiments were carried out at illumination intensities and exposure times which are typical for epifluorescence imaging. The effect was even more prominent in a confocal microscopy setup using laser excitation at 458 nm (0.2−1 mW; data not shown). Classical irreversible photobleaching is common among fluorescent proteins (*1*), but several observations indicated that it was not responsible for this effect. First, the fluorescence intensity decreased only during the first 4−6 illumination cycles and reached a stable level afterward, whereas irreversible photobleaching should result in an ongoing exponential decay of the fluorescence intensity. Second, the observed photobleaching was reversible: if the sample was kept in the dark for 100 s, the fluorescence recovered almost to the initial intensities (Figure 1c, upper panel). Third, additional illumination of the sample exerted further wavelength-dependent effects on the fluorescence intensity. For example, illumination of the sample at 500

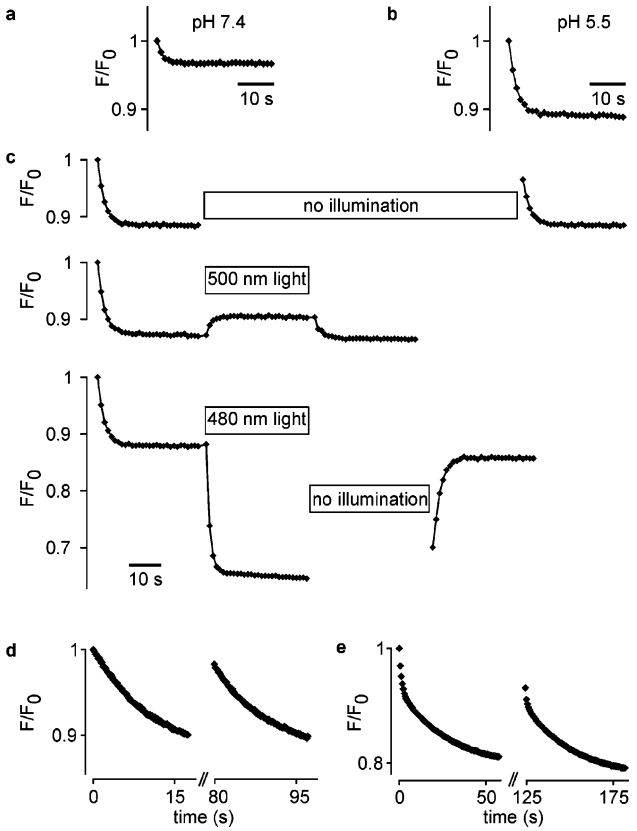


FIGURE 1: Reversible photobleaching of eCFP. (a) HEK 293 cells expressing eCFP were kept in the dark and then imaged by brief 430 nm pulses (10 ms). (b) Same experiment as in part a, but cells were equilibrated to pH 5.5 in the presence of nigericine (10 $\mu$M) prior to imaging. (c) Same experimental setting as in part b, but the protocol was modified to include dark intervals or intervals with additional illumination at 500/480 nm between the image acquisition (1 s per frame) as indicated by the boxes. Illumination intensities were 0.48, 0.64, and 0.59 W cm$^{-2}$ at 430, 480, and 500 nm, respectively. (d) Reversible photobleaching was performed on a droplet (diameter: 500 $\mu$m) of a solution of purified eCFP at pH 7.0 under mineral oil by applying 460 nm light (0.025 W cm$^{-2}$) using a 10×/0.5 Fluar objective. Between the two depicted bleach cycles, samples were kept in the dark. (e) The same experiment as in part d for purified Citrine at pH 6.0, bleached at 420 nm (0.057 W cm$^{-2}$).

nm (applied between imaging cycles) resulted in a partial recovery of the fluorescence intensity (Figure 1c, middle panel), whereas illumination at 480 nm led to a further, but still reversible, decrease in the fluorescence intensity (Figure 1c, lower panel). Of note, the slow recovery in the dark was markedly accelerated by continuing the image acquisition and thereby illuminating the probe at 430 nm for 10 ms per frame to reestablish a steady-state fluorescence intensity similar to that before applying the 480 nm light (Figure 1c, lower panel). Thus, the observed effect represents a previously uncharacterized reversible photobleaching and a spontaneous or light-accelerated recovery of eCFP. A similar reversible photobleaching was also observed for eYFP and Citrine (see below) as well as for eGFP (data not shown). For all examined GFP color variants, reversible photobleaching was more pronounced under acidic conditions (see for example Figure 1a,b).

Reversible photobleaching was observed not only in living cells expressing the respective GFP variant but also on purified eCFP, eYFP, or Citrine (Figure 1d,e). Thus, the observed effects are intrinsic properties of the GFP color variants.

*Spontaneous and Light-Induced Recovery of Reversibly Photobleached GFP Variants.* The fluorescence of reversibly bleached eCFP spontaneously recovered in the dark (Figure 2a). The recovery kinetics could be fitted to a monoexponential growth function $F = F_{max}(1 - e^{-kt})$ yielding a time constant of $\tau = 1/k = 58$ s. Experiments with eYFP and Citrine yielded time constants of $\tau = 54$ s and $\tau = 25$ s, respectively. Similar time courses were measured for purified proteins (data not shown). Short illumination times at 430 nm, which are typically used to excite eCFP in imaging applications, substantially accelerated the recovery of reversibly bleached eCFP (Figure 2b). These results indicate that 430 nm light exerts a dual effect on eCFP by inducing a reversible photobleach as well as by accelerating the recovery of reversibly bleached eCFP. Likewise, illumination at 500 nm accelerated this recovery (Figure 2c), but was less effective in inducing reversible photobleaching.

*Photobleaching and Absorption Spectra of GFP Color Variants.* Reversible photobleaching spectra were obtained by determining the spontaneous recovery of fluorescence intensities during a 60 s dark interval (Figure 3a). Reversible photobleaching of the yellow color variants was most effective at 400−440 nm (Figure 3b). In this spectral range, however, the absorption of these fluorescent proteins at neutral pH is minimal (*14*, *15*). At acidic pH, Citrine displays an absorption band around 412 nm (*15*). Thus, we recorded absorption spectra of purified eYFP, Citrine, and eCFP at various pH values to compare them to the spectral properties of reversible photobleaching (Figure 3c). Indeed, both eYFP and Citrine displayed significant absorption at 400−440 nm at acidic pH, which, however, did not result in fluorescence emission (data not shown). The absorption spectra recorded at different pH values displayed isosbestic points at 449 and 439 nm for Citrine and eYFP, respectively. For eCFP, the reversible photobleaching spectrum is in good agreement with the measured absorption spectrum, which exhibited only minor pH dependence (Figure 3b,c).

*A Kinetic Model for Reversible and Irreversible Photobleaching.* Due to its spectral properties, the reversible photobleaching during an experiment is always confounded

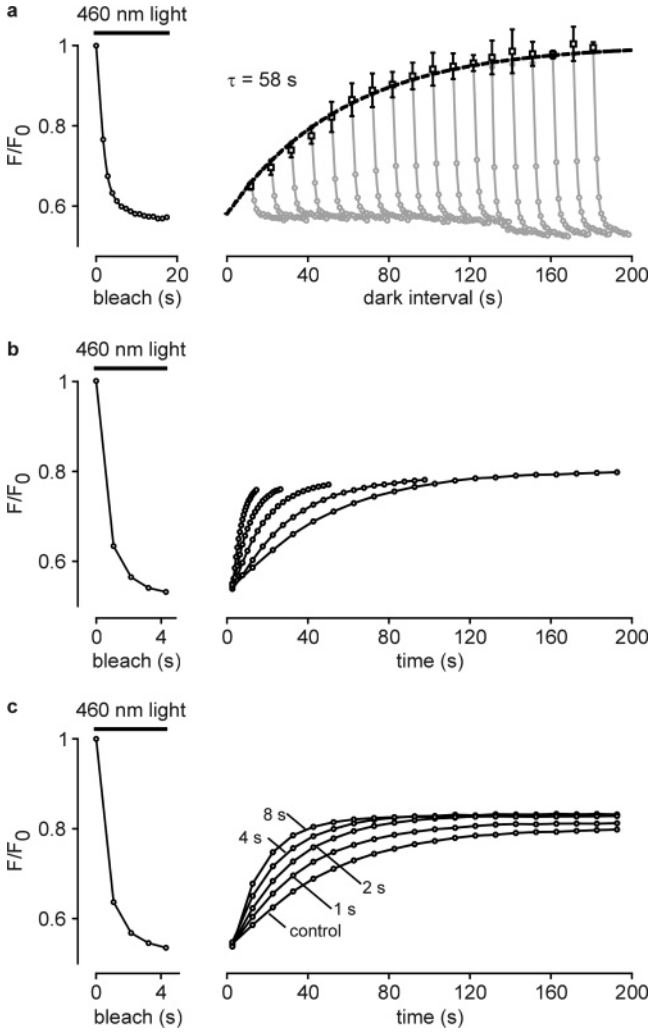


FIGURE 2: Spontaneous and light-induced recovery of reversibly bleached eCFP. (a−c) HEK 293 cells expressing eCFP were analyzed by fluorescence imaging at $pH_i = 5.5$. eCFP was reversibly photobleached by 460 nm light (0.56 W $cm^{-2}$) as indicated by the bars. (a) After photobleaching, samples were kept in the dark for 10 to 180 s and then again subjected to a second cycle of reversible photobleaching (gray symbols and lines). Data of 18 experiments with different dark intervals are superimposed. The initial intensity after the dark interval was determined in 3 independent experiments, and means ± SD are shown (open squares). The amount of spontaneous recovery was plotted as a function of the dark interval duration and fitted to a monoexponential rise-to-maximum function (dashed line) to assess the time constant of spontaneous recovery. (b) After reversible photobleaching, fluorescence images ($\lambda_{ex} = 430$ nm; 0.48 W $cm^{-2}$, 10 ms illumination per frame) were collected at various acquisition frequencies (0.1−1.6 $s^{-1}$) to track the recovery process. (c) Images were acquired as in part b at 10 s intervals. During each interval, no illumination (control) or 500 nm light (1, 2, 4, or 8 s per cycle, 0.59 W $cm^{-2}$) was applied.

to a variable degree by irreversible photobleaching. To dissect reversible and irreversible components of the photobleaching kinetics, we developed a simplified kinetic model to which we could fit the photobleaching data.

Typical fluorescence decay kinetics involving reversible and irreversible photobleaching consist of two phases (see for example Figure 1a−c): an initial phase in which the rapid reversible photobleaching leads to a fast decay of the fluorescence intensity, and a second phase which is dominated by a more slowly ongoing irreversible photobleaching. The most simple model which can describe this process considers the reversible transitions of a fluorescent protein

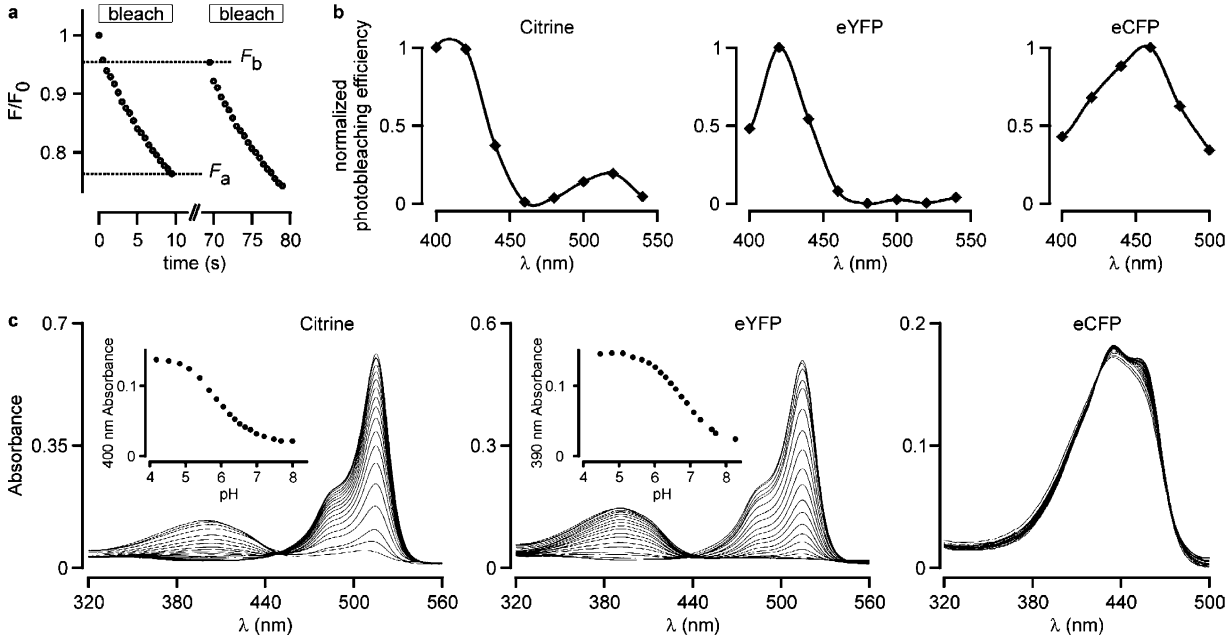


FIGURE 3: Comparison of reversible photobleaching and absorption spectra. (a, b) Reversible photobleaching spectra were determined in HEK 293 cells expressing Citrine, eYFP, or eCFP, respectively, at physiological pH. (a) Demonstration of the experimental protocol. For each wavelength, the respective GFP variant (here: Citrine) which was previously kept in the dark was bleached by 500 ms pulses at the respective wavelength (here: $\lambda = 400$ nm). After a cycle of 20 bleaching pulses, no illumination was applied for 60 s to allow reversibly bleached fluorescent proteins to recover. Then, a second bleaching cycle was performed. The minimal fluorescence of the first bleaching cycle was denoted as $F_a$, and the maximal fluorescence of the second bleaching cycle was denoted as $F_b$. The extent of reversible photobleaching at that wavelength is then given as $F_b - F_a$. Fluorescence was measured by short pulses of 10 ms at the respective excitation optimum. (b) Normalized reversible photobleaching spectra of Citrine, eYFP, and eCFP, corrected for the lamp intensity profile and background. (c) Absorption spectra of purified Citrine, eYFP, and eCFP, recorded at different pH ranging from 9.2 to 4.2 (down from the top at 514 nm for Citrine, eYFP, and at 455 nm for eCFP). Insets show the absorption at 400 or 390 nm for Citrine or eYFP, respectively, plotted against pH.

between a native state ($FP_{nat}$) and a reversibly bleached state ($FP_{rbl}$) described by the rate constants $k_1$ and $k_2$, and a transition of $FP_{nat}$ to an irreversibly bleached state ($FP_{ibl}$) with a rate constant $k_3$ (see Figure 4a). If we assume first-order kinetics for all three transitions, the system is described by the following system of differential equations:

$$d[FP_{nat}]/dt = -(k_1 + k_3)[FP_{nat}] + k_2[FP_{rbl}]$$

$$d[FP_{rbl}]/dt = -k_2[FP_{rbl}] + k_1[FP_{nat}]$$

Assuming the initial conditions $[FP_{nat}] = 1$, $[FP_{rbl}] = 0$, and $[FP_{ibl}] = 0$, the rate constant of reversible photobleaching ($k_1$) indeed corresponds to the velocity of the initial phase, while the fluorescence level in the equilibrium phase is determined by the ratio between $k_1$ and the rate constant of the reverse reaction ($k_2$). The rate constant of irreversible photobleaching ($k_3$) determines the velocity of the ongoing fluorescence decay in the equilibrium phase.

We performed photobleaching experiments at the optimal wavelengths for reversible photobleaching. At these wavelengths, the experimental data were in good agreement with a fit to the analytical solution of the differential equations (Figure 4b,c). The obtained rate constants are given in Table 1. The predicted fractions for irreversibly and reversibly bleached molecules were further confirmed by measuring the fluorescence after a dark relaxation period, showing recovery to an extent similar to that predicted by the model (see Figure 4b,c). The photobleaching kinetics of eYFP was similar to that of Citrine, but with slower rate constants for reversible as well as irreversible photobleaching (see Table 1).

The ratio of the probabilities of reversible and irreversible photobleaching ($P_{rbl}/P_{ibl}$) could be determined independently of the model by dividing the fractional bleaching during the first two frames, which at the optimal wavelengths for reversible photobleaching was caused almost exclusively by reversible photobleaching, by the fractional bleaching per frame during the equilibrium phase, which mostly represents irreversible photobleaching. The results are given in Table 1 showing that the probability of reversible photobleaching was 67- to 168-fold greater than that for irreversible photobleaching if the fluorescent proteins were illuminated at the optimal wavelengths for reversible photobleaching.

By using the determined rate constants for reversible photobleaching ($k_1$), we could calculate the quantum efficiencies of reversible photobleaching ($\phi_{rbl}$) as $(I\epsilon t_{90\%})^{-1}$ (*16*), where $I$ is the irradiation intensity in einsteins $cm^{-2}$ $s^{-1}$, $\epsilon$ is the extinction coefficient in $cm^2$ $mol^{-1}$, and $t_{90\%}$ is given as $k_1^{-1}$ ln(10) (see Table 1). Absorption coefficients of the protonated state adapted to the actual fraction of protonated molecules at pH 7.2 were used. The calculated quantum efficiencies are surprisingly high. For example, the quantum efficiency of reversible photobleaching of Citrine at 420 nm (see Table 1) is about 270-fold higher than the quantum efficiency of irreversible photobleaching at 490 nm (*6*).

*Dependence of Reversible Photobleaching of eCFP on the Illumination Intensity and the Presence of a FRET Acceptor.* To more precisely define the possible mechanism underlying the reversible photobleaching of eCFP, we examined the dependence of the reversible photobleaching rate on the illumination intensity. A linear dependence would implicate that the reversible photobleaching was initiated by interaction

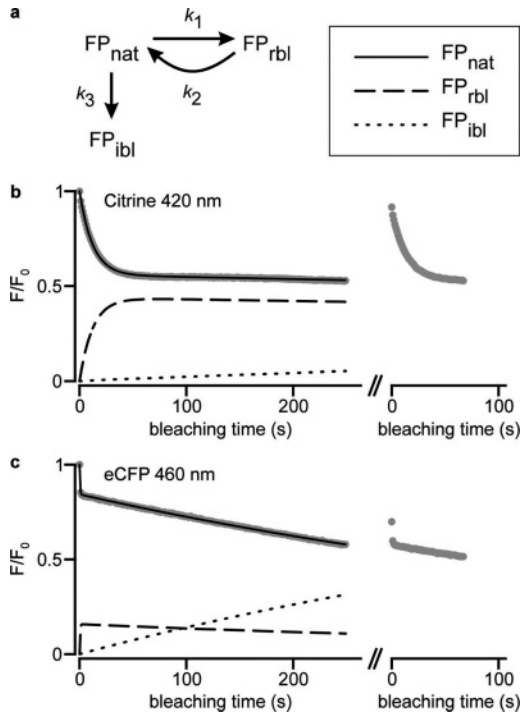


FIGURE 4: A kinetic model for photobleaching of GFP variants. (a) The kinetic model used to interpret photobleaching data of GFP variants. (b, c) Photobleaching experiments were performed on Citrine- or eCFP-expressing HEK 293 cells. In a first cycle, the cells were bleached by 250 pulses of 1 s illumination at the indicated wavelength. Then, a dark interval of 120 s was applied to allow reversibly bleached fluorescent proteins to recover. After the dark interval, a second photobleaching cycle was applied to demonstrate the partial recovery of the reversibly bleached fraction (right panels). Rate constants used in the kinetic model were then obtained by nonlinear least-squares regression analysis of the fluorescence time course during the first bleaching cycle. Depicted are experimental data (gray traces) and the calculated values for $FP_{nat}$ (solid line), $FP_{rbl}$ (dashed line), and $FP_{ibl}$ (dotted line) from the best fit. (b) Citrine was bleached at 420 nm. (c) eCFP was bleached at 460 nm. Light intensities were 2.35, 3.5, and 2.5 W $cm^{-2}$ at 420, 460, and 514 nm, respectively.

Table 1: Data Obtained from Reversible Photobleaching Experiments

| | eCFP | eYFP | Citrine |
|---|---|---|---|
| $\lambda$ (nm)[a] | 460 | 420 | 420 |
| $k_1$ ($s^{-1}$)[b] | 0.40 | $7.7 \times 10^{-3}$ | $3.6 \times 10^{-2}$ |
| $k_2$ ($s^{-1}$)[b] | 2.15 | $1.6 \times 10^{-2}$ | $4.6 \times 10^{-2}$ |
| $k_3$ ($s^{-1}$)[b] | $1.7 \times 10^{-4}$ | $1.4 \times 10^{-4}$ | $3.7 \times 10^{-4}$ |
| $P_{rbl}/P_{ibl}$[c] | 129 | 67 | 168 |
| $F_{prot}$[d] | $8.9 \times 10^{-2}$ | 0.1 | $3.2 \times 10^{-2}$ |
| $I$ (einsteins $cm^{-2}$ $s^{-1}$)[e] | $1.34 \times 10^{-5}$ | $8.3 \times 10^{-6}$ | $8.3 \times 10^{-6}$ |
| $\epsilon$ ($cm^2$ $mol^{-1}$)[f] | $2.8 \times 10^7$ | $1.37 \times 10^7$ | $1.41 \times 10^7$ |
| $\phi_{rbl}$[g] | $5.19 \times 10^{-3}$ | $3.03 \times 10^{-4}$ | $4.24 \times 10^{-3}$ |

[a] Photobleaching wavelength. [b] The rate constants obtained by fitting the photobleaching data to the kinetic model. [c] The ratio of the probabilities for reversible and irreversible photobleaching at the given wavelength. [d] The protonated fraction at pH 7.2. [e] Irradiation intensity. [f] Extinction coefficient. [g] The quantum efficiency of reversible photobleaching.

of photons with a ground state of the chromophore, while a supralinear dependence would be expected if reversible photobleaching was caused by interaction of photons with an excited state. We performed reversible photobleaching experiments with eCFP, in which we varied the illumination intensity by placing a pair of crossed polarizers at different

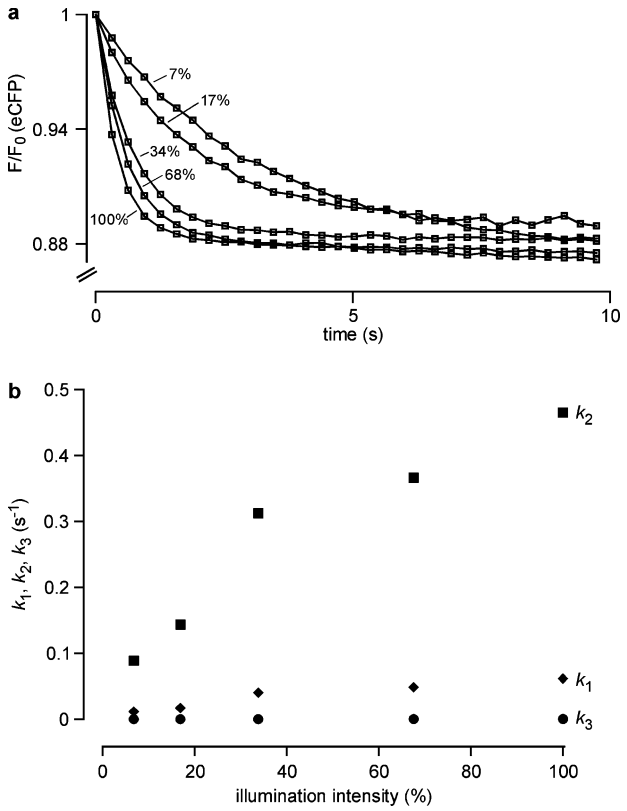


FIGURE 5: Dependence of the photobleaching kinetics of eCFP on the illumination intensity. Photobleaching experiments were performed on eCFP-expressing HEK 293 cells by applying 250 ms illumination at 460 nm every 314 ms. The illumination intensity was modulated by varying the angle between a pair of polarizers in the excitation pathway. (a) The time courses of the eCFP fluorescence at 5 different illumination intensities as indicated are shown. (b) At each illumination intensity, the photobleaching data were fitted to the kinetic model as described in the main text. The obtained rate constants $k_1$, $k_2$, and $k_3$ are shown as a function of the illumination intensity. The illumination intensity at 100% was 0.62 W $cm^{-2}$.

angles in the excitation pathway (Figure 5). The photobleaching kinetics at each illumination intensity (see Figure 5a) were analyzed by curve-fitting using the simplified kinetic model described above. The resulting rate constants $k_1$, $k_2$, and $k_3$ are given in Figure 5b. The rate constants for reversible photobleaching ($k_1$) and the reverse reaction ($k_2$) showed a linear dependence on the illumination intensity, implicating that reversible photobleaching originates from an interaction of photons with the ground state of the chromophore and is a single-photon process.

Irreversible photobleaching of eCFP is slower in the presence of a closely positioned acceptor fluorochrome such as eYFP, because both irreversible photobleaching and fluorescence resonance energy transfer (FRET) are competitive inactivation pathways for the excited state of the eCFP chromophore (*2*). To test whether reversible photobleaching is also a possible inactivation pathway for this excited state, we performed reversible photobleaching experiments using eCFP under two different conditions (Figure 6): eCFP coexpressed with eYFP in the same cell, or a eCFP-eYFP tandem protein exhibiting a FRET efficiency of about 50% (*17*). Indeed, the initial fluorescence decay was slower in the eCFP-eYFP tandem protein as compared to the separately expressed fluorescent proteins, and the fluorescence intensity

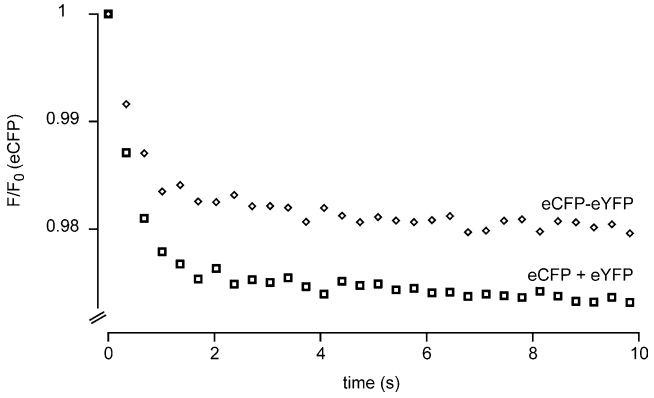


FIGURE 6: Dependence of the photobleaching kinetics of eCFP on the presence of a FRET acceptor. Photobleaching experiments were performed on HEK 293 cells transfected with plasmids encoding either eCFP and eYFP (eCFP + eYFP) or a tandem protein in which eCFP was directly fused to eYFP (eCFP-eYFP). Every 339 ms, the fluorescence intensities of eCFP and eYFP were determined separately by 50 ms excitation at 430 nm and 10 ms excitation at 520 nm, respectively. The fluorescence of eCFP, which was corrected for acceptor photobleaching by assuming FRET efficiencies of 0% (eCFP + eYFP) or 50% (eCFP-eYFP), is shown. Illumination intensities were 0.64 W $cm^{-2}$ and 0.49 W $cm^{-2}$ at 430 and 520 nm, respectively.

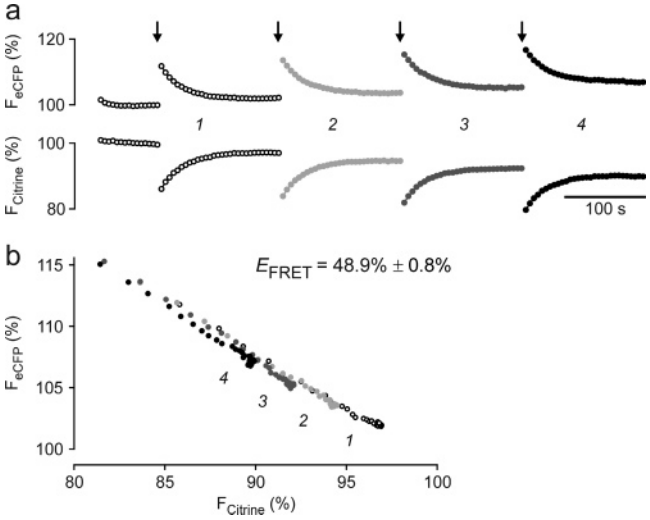


FIGURE 7: Transient unquenching of a FRET donor by reversible photobleaching of the acceptor. HEK 293 cells expressing a eCFP-Citrine fusion protein-expressing were analyzed by fluorescence imaging. Images were acquired every 5 s at 440 and 500 nm excitation with 10 and 6 ms illumination times for eCFP and Citrine, respectively. (a) Time courses of the fluorescence intensities of eCFP (upper panel) and Citrine (lower panel) are depicted. At four time points (denoted as 1−4), Citrine was reversibly photobleached by a 5 s illumination at 400 nm (as indicated by the arrows), and fluorescence intensities of eCFP and Citrine during subsequent recovery of Citrine were recorded. Light intensities were 0.67, 1.18, and 1.61 W $cm^{-2}$ at 400, 440, and 500 nm, respectively. (b) The correlation between fluorescence intensities of eCFP and Citrine during spontaneous recovery of Citrine is depicted for each acceptor bleaching experiment (1−4). Linear regression analysis served to extrapolate the donor fluorescence at 100% ($F_{DA}$) and 0% ($F_D$) acceptor intensity for each relaxation process, and the calculated FRET Efficiency ($E_{FRET}$) is given as mean ± SEM.

in the equilibrium phase was higher. These data indicate that the reversibly bleached state of eCFP is reached by an inactivation pathway of an excited state which may also inactivate via FRET to a closely positioned eYFP. However, on the basis of these data, it cannot be decided whether this is the same excited state which is involved in fluorescence emission.

*Reversibly Bleached Citrine Is Characterized by a Reduced Absorbance.* A fluorescent protein may appear bleached because of a reduced absorbance, or because of a reduced fluorescence quantum yield. The common irreversible photobleaching of fluorescent molecules is usually attributed to an irreversible destruction of their chromophores, leading to a loss of absorbance. The common method for measuring FRET by irreversible photobleaching of the acceptor, which leads to unquenching of the donor fluorescence, relies on this light-induced loss of absorbance. To test whether the reversible photobleaching of GFP variants is also caused by a temporary reduction of their absorbance, we performed reversible photobleaching on Citrine located in an eCFP-Citrine tandem fusion protein, in which the close proximity of the two chromophores causes a FRET efficiency of 46−52% (*17*).

Indeed, in this construct, reversible photobleaching of Citrine by about 13% led to a transient increase in the measured eCFP fluorescence by about 12% (Figure 7a,b). Both effects reversed with half-times corresponding to the typical spontaneous recovery kinetics of Citrine, indicating that indeed reversibly photobleached Citrine is responsible for the inverse changes of fluorescence intensity in the CFP emission band. Moreover, this effect was also observed in the eCFP-eYFP tandem protein (although with a lower efficiency; data not shown), and this procedure could be repeated several times. We conclude that reversible photobleaching of the FRET acceptors Citrine or eYFP represents a true reduction of their respective absorbance thereby affecting the spectral overlap between eCFP fluorescence and Citrine or eYFP absorbance. In cells expressing only eCFP, application of the bleaching pulses had no significant effect on eCFP fluorescence (data not shown). The calculated FRET efficiency of 48.9% was in good agreement with that measured by conventional irreversible acceptor photobleaching (data not shown). This suggests that reversible photobleaching of Citrine reflects a transient loss of its absorbance at wavelengths contributing to the spectral overlap integral with eCFP emission.

Because of the rapid spontaneous recovery of Citrine from reversible photobleaching, the observed reversible unquenching of the donor fluorescence might be useful as a nondestructive method for measuring FRET efficiencies, since it allows repetitive quantitative determinations of the FRET efficiency (see Figure 7). In contrast to emission-ratio imaging, this method is independent of the actual steady-state fluorescence of eCFP and, thus, allows for spatially resolved repetitive and quantitative analyses of conformational changes and dynamic protein−protein interactions. Thus, it could serve as a valuable tool for quantitative and time-resolved analyses of second messenger formation, protein phosphorylation, protease/caspase activity, or other dynamic processes which have been visualized by FRET-based sensor proteins (*18*).

*Implications for FRET Microscopy—Donor Photobleaching Lifetime.* A donor fluorochrome may escape photobleaching by transferring its excited-state energy to a closely positioned acceptor via FRET (*19*−*21*). Therefore, the resulting delay of the donor photobleaching kinetics can be

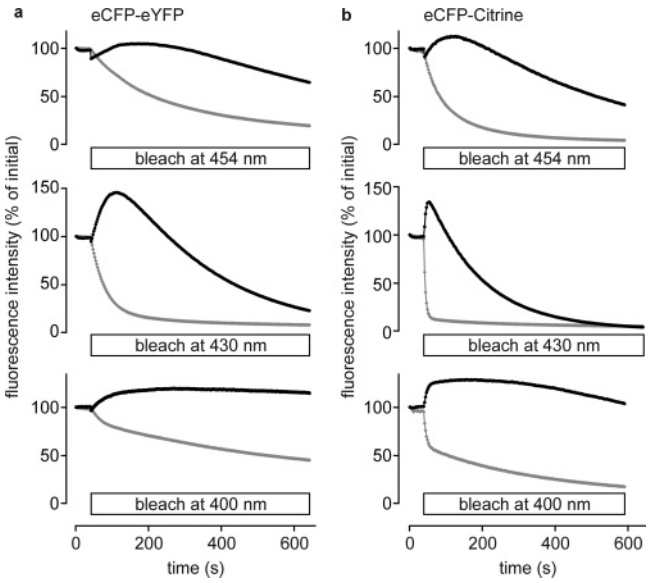


FIGURE 8: Donor photobleaching lifetime experiments with fluorescent tandem proteins. Donor photobleaching experiments were performed on HEK 293 cells transfected with plasmids encoding eCFP-eYFP (a) or eCFP−Citrine (b). Donor and acceptor fluorescences were recorded separately, using 8 ms of illumination for each image. After a baseline of 15 imaging cycles, an additional 2200 ms illumination at the indicated photobleaching wavelength was applied between each of the following imaging cycles. The donor (black traces) and acceptor (gray traces) fluorescence intensities are shown. Illumination intensities were 1.1, 1.4, and 1.5 W $cm^{-2}$ at 400, 430, and 454 nm, respectively. Note the paradoxical increase in donor intensities which result from both reversible and irreversible acceptor cross-bleach.

used to detect FRET between fluorochrome-labeled antibodies (*19*−*22*) or between eCFP- and eYFP-fused proteins (*23, 24*). Since we observed reversible photobleaching of eYFP and Citrine upon illumination at 400−440 nm (see Figure 3), we wondered whether eCFP can be selectively photobleached without disturbing the yellow acceptor fluorochromes. In cells expressing either eCFP-eYFP tandem or eCFP-Citrine tandem, eCFP could not be photobleached without affecting the FRET acceptor. At the excitation maximum of eCFP (454 nm), eYFP or Citrine was cross-bleached more rapidly than eCFP itself. Since we were investigating tandem proteins that exhibit a FRET efficiency of about 50%, this acceptor cross-bleach even led to a transient increase in donor fluorescence (Figure 8a,b, upper panel). Likewise, if excited at 458 nm with an argon laser, eYFP was photobleached about 4-fold faster than the intramolecularly linked eCFP as tested with a spectrally resolving confocal microscope (LSM-META, Carl Zeiss, data not shown). To reduce the acceptor cross-excitation, eCFP may be photobleached at 430−440 nm. Under these conditions, however, the donor photobleaching kinetics was even more severely affected by reversible eYFP photobleaching (Figure 8a,b, middle panel). At the local fluorescence excitation minimum of eYFP and Citrine (400 nm), reversible photobleaching of the acceptor still exceeded the donor photobleaching (Figure 8a,b, lower panel). The resulting kinetics of the donor fluorescence, thus, reflects a complex superposition of reversible and irreversible photobleaching of the donor as well as reversible and irreversible photobleaching of the acceptor, causing partial donor recovery. Thus, paradoxically, protocols designed to selectively bleach the donor initially led to an increase in the donor fluorescence, and a monoexponential decay of the donor fluorescence did not establish until the acceptor fluorescence was almost completely bleached. Evaluation of donor photobleaching lifetimes is, therefore, not applicable to quantify FRET between these fluorescent proteins. Moreover, the transient unquenching of donor fluorescence observed in these experiments corroborates the finding that reversible photobleaching of the acceptor fluorescent proteins not only is caused by a reduction of their fluorescence quantum yield but also reflects a transient reduction of their absorbance in the spectral range of eCFP emission.

The aforementioned data were acquired with intramolecularly linked fusion proteins exhibiting FRET efficiencies of about 50%. Under these conditions, the FRET acceptor may be bleached not only by direct excitation but also via FRET-mediated energy uptake. To test the latter hypothesis, we performed donor photobleaching experiments with a eCFP-PKC$\epsilon$-eYFP fusion protein exhibiting a typical FRET efficiency of only 7.2%. Indeed, applying identical experimental settings, eYFP located in the eCFP-PKC$\epsilon$-eYFP fusion protein was less efficiently and more slowly photobleached at 430 nm than the same acceptor located within the eCFP-eYFP tandem (data not shown). Since direct excitation of the eYFP component should be identical in both proteins, we conclude that the closely positioned donor in eCFP-eYFP supplies additional energy causing photobleach via FRET. A similar FRET-sensitized acceptor photobleaching has previously been described for energy transfer between synthetic fluorochromes (*25*).

*Spontaneous and Light-Induced Recovery of Reversibly Bleached eCFP Mimicks FRAP.* The reversible photobleaching described here can severely affect cell biological experiments even at physiological pH. For example, FRAP experiments rely on the assumption that locally bleached fluorescence is replenished by laterally moving unbleached molecules. However, we have shown that eCFP can be reversibly photobleached at its absorption maximum and recovers either spontaneously or in a light-accelerated fashion. We, thus, tested whether FRAP assays applying this GFP variant may be distorted by recovery from a reversibly bleached state. We have previously shown that the human TRPC4$\alpha$ ion channel is arranged in immobile clusters within the plasma membrane of HEK 293 cells (Figure 9a, ref *26*). FRAP analysis revealed a poor mobility of TRPC4$\alpha$-YFP within these clusters (5.5% recovery with a time constant of 0.6 s; Figure 9b). A parallel determination using TRPC4$\alpha$-eCFP in the same channel cluster, however, revealed a substantially stronger fluorescence recovery (65.9% recovery with a time constant of 0.36 s, see Figure 9b). Since TRPC4$\alpha$-eCFP forms multimeric channel complexes with TRPC4$\alpha$-eYFP (*26*), a differential mobility of both proteins is unlikely. We conclude that FRAP assays with eCFP-fused proteins may be significantly distorted by spontaneous and light-induced recovery of the reversibly bleached fluorochrome.

## DISCUSSION

*A Tentative Mechanism for Reversible Photobleaching.* Our data provide some insight into the possible mechanism of the observed reversible photobleaching of GFP variants.

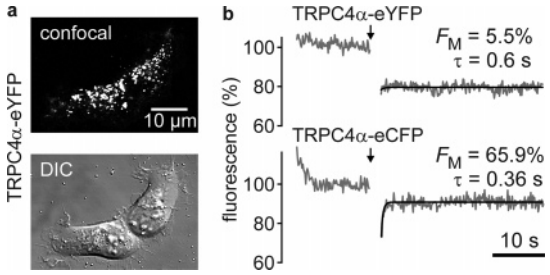


FIGURE 9: Recovery of reversibly bleached eCFP mimicks FRAP. Fluorescence recovery after photobleaching (FRAP) experiments were performed on HEK 293 cells expressing both TRPC4α-eCFP and TRPC4α-eYFP using a confocal laser scanning microscope (LSM-META, Carl Zeiss). FRAP was assayed sequentially for eYFP- and eCFP-fused proteins over the same region of interest. Fluorescent proteins were excited with the 458 nm (eCFP) or the 514 nm (eYFP) lines of an argon laser combined with appropriate dichroic mirrors and 470−500 nm (eCFP) and 530−560 nm (eYFP) band-pass emission filters. The fluorescence over a predefined region was imaged before and after brief photobleaching by pulses of maximal laser energy. (a) Confocal image of TRPC4α-eYFP (upper panel) and differential interference contrast (DIC) image of the same cells (lower panel). (b) Time courses of the fluorescence intensities of eYFP and eCFP during FRAP experiments are depicted as gray lines. After recording a baseline, a region over a fluorescent cluster was bleached by repetitive scanning at maximal laser intensity (indicated by the arrows). The kinetics of the subsequent fluorescence recovery was fitted by a monoexponential recovery function (black line) to obtain the recovery time constant $\tau$ and the mobile fraction $F_M$.

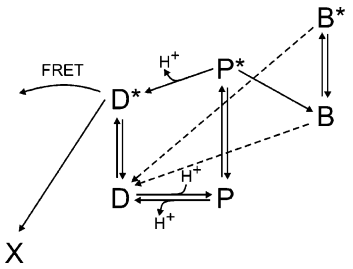


FIGURE 10: A model describing the possible transitions of a fluorescent protein between fluorescent, protonated, and reversibly bleached states. The model considers a protonated form (**P**), a deprotonated form (**D**), and a reversibly bleached form (**B**) of the fluorescent protein which can each exist in ground and excited states, as well as an irreversibly bleached state **X** (details are given in the main text).

A model describing the possible transitions between fluorescent, protonated, and reversibly bleached states which is consistent with our data is shown in Figure 10. The pH-dependent absorption spectra of the yellow color variants result from two distinct states: a protonated state (**P**) and a deprotonated state (**D**) which coexist in a pH-dependent equilibrium **(P ↔ D)**. Analysis of a pH-dependent flickering which was observed in fluorescence correlation spectroscopy studies performed on eGFP showed that protonation reactions of the chromophore occur on the microsecond time scale (*27*). Considering the pH-dependent partial quenching of the eCFP fluorescence (*17*) and the modest, but reproducible, changes in the absorption spectra (see Figure 3), such a protonation equilibrium may also exist for this color variant. In the yellow variants, the decisive protonation may be located at the phenolic acid of the chromophore as described for the wild-type GFP (*1*, *27*). In eCFP, this phenolic acid is replaced by an indole ring system. However, since reversible photobleaching of eCFP was again more efficient at acidic pH, protonation of a site other than the chromophore must be involved. Moreover, it is possible that also in the yellow variants the protonation sensitizing the protein for reversible photobleaching is not identical to the protonation of the chromophore but only occurs at a similar p$K_a$.

Analysis of the protein environment of the chromophore points to three titratable residues in the vicinity of the chromophore. Glu222 is located close to the imidazolinone part of the chromophore, allowing hydrogen bond interactions between the glutamate oxygens and the nitrogen of the imidazolinone ring system. Decarboxylation of this residue was implicated in the irreversible photoconversion of GFP to a 483-nm-absorbing species (*4*), showing that it significantly interacts with the chromophore and influences its optical properties. However, the glutamate side chain is deeply buried within the protein environment and may not be notably influenced by changes in solution pH, although the decarboxylated Glu222 has been supposed to accept a proton from the chromophore phenol (*4*).

Tyr145 and His148 are more accessible for protons from the solution and are, thus, more likely candidates for the protonation leading to enhanced susceptibility to reversible photobleaching. Tyr145 and His148 are both suitably located to establish a hydrogen bond to the phenolic acid of the chromophore in yellow variants. The more acidic p$K_a$ value of histidine is in good agreement with our observations that reversible photobleaching occurs at neutral and acidic pH. The highly basic p$K_a$ of the tyrosine phenolic acid indicates that it should remain protonated even at basic solution pH, if its p$K_a$ is not considerably shifted by the protein environment.

In eCFP, X-ray crystallogaphic studies have shown two different conformations of Tyr145 and His148, which coexist and may explain the two absorption bands of eCFP (*28*). Although, in eCFP, His148 is unable to form a hydrogen bond with the chromophore, the change in electrostatic potential of the chromophore environment brought about by protonation of His148 may still influence the chromophore properties in a way which favors reversible photobleaching. Moreover, changes in protonation of these two residues may also influence the equilibrium between both conformations of eCFP, which may further modulate its susceptibility to reversible photobleaching.

The classical fluorescence cycle originates from excitation of the deprotonated ground state **D**. Alternative relaxation routes for this excited state are fluorescence resonance energy transfer to a closely positioned acceptor chromophore and irreversible photobleaching, which leads to a nonfluorescent species **(P* → X)** with quantum efficiencies of about $10^{-6}$ to $10^{-5}$ (*6*, *8*). We have shown that illumination of the yellow color variants in the spectral range of their protonated forms results in reversible photobleaching (see Figure 3). In addition, the linear dependency of the reversible photobleaching rate on the illumination intensity (see Figure 5) implies that this reversible photobleaching arises from interaction of photons with a ground state, presumably the protonated ground state (**P**). Absorption of a photon may lead to the generation of an excited state (**P → P***), which may then relax to the reversibly bleached state (**P* → B**). We provide reversible photobleaching spectra which presumably represent the excitation spectra of this excited state (see Figure 3), which depopulates toward a reversibly bleached

state with quantum efficiencies more than 100 times greater than those of irreversible photobleaching (*6, 8*).

Alternatively, the excited protonated state **P*** might first deprotonate **(P* → D*)** as described for wild-type GFP (*1*). However, at least in the yellow variants, such an excited-state proton transfer is unlikely, since under these circumstances one would expect similar reversible photobleaching rates regardless of the pH and the excitation wavelength. Moreover, the fluoresence excitation spectra of eYFP and Citrine have local minima in the spectral range of the absorption of their protonated forms (data not shown), indicating that an excited-state proton transfer does not occur in these color variants.

In eCFP, an excited-state transition **P* → D*** might indeed occur, which could explain why the fluorescence emission of this color variant drops by only 40% upon protonation (ref *17*, see Figure 3). The observation that the reversible photobleaching rate of CFP is slower in the presence of a closely positioned eYFP (see Figure 6) could also be explained by such a transition, since it is well-known that the excited deprotonated state **D*** of eCFP can relax via FRET to eYFP (*17*), a mechanism which might compete with the generation of the reversibly bleached state. However, another explanation for this competition between radiationless energy transfer and reversible photobleaching would be that the transition energy for the excitation of the protonated and deprotonated states of eCFP is similar and, thus, both excited states are able to inactivate by FRET to eYFP. This is likely, because the absorption spectrum of eCFP is not very sensitive to pH changes (see Figure 3).

The reversibly bleached state **B** may return into a fluorescent state by more than one way. First, we have shown that reversibly bleached fluorescent proteins regain their fluorescence in the dark with time constants of several seconds (see Figure 2a). Because of the fast equilibrium **P ↔ D**, it cannot be decided whether the reversibly bleached state relaxes directly to the fluorescent deprotonated ground state (**B → D)** or via one of the states **P**, **P***, or **D***.

Second, the restoration of fluorescence can be accelerated by illumination (see Figure 2b,c). This implicates the absorption of a photon by the reversibly bleached state, which presumably leads to the generation of another excited state **(B → B*)** which serves as a gateway to more rapidly relax back to the fluorescent ground state. Again, on the basis of our data, it cannot be decided if the excited reversibly bleached state **B*** relaxes to the deprotonated ground state **(B* → D)** or to a different state which is in fast equilibrium with **D**. However, our data allow some speculations about the properties of the state **B**: The reversibly bleached eCFP effectively regained its fluorescence upon illumination at 500 nm (see Figure 2c). This implies that the absorption spectrum of **B** may be red-shifted as compared to **D** or **P**. For the yellow variants, however, we do not know if the reversibly bleached state is still capable of absorbing photons. It has been reported that several variants of the green fluorescent protein undergo red shifts of their absorption and emission spectra upon strong illumination under conditions of low oxygen concentration (*29*). It may be speculated that these long-lived red-shifted states correspond to reversibly bleached states described herein, which would imply that the reversibly bleached states require oxygen to regain fluorescence.

The reversible photobleaching described in this study differs from irreversible processes such as the photochromism of wild-type GFP (*4, 30*) or the photoactivation of a fluorescent protein (*31*). At the single-molecule level, reversible photobleaching would appear as blinking or flickering. A slow blinking has been described for polyacrylamide-embedded single YFP and eGFP molecules excited at 488−514 nm (*7, 32*). Interestingly, the light-induced reactivation described for the yellow fluorescent T203F variant occurs at 405 nm, a wavelength that was maximally effective in reversibly photobleaching eYFP or Citrine (see Figure 3). In addition, effects of acidic pH on the slow single-molecule blinking have not been reported. Fluorescence correlation spectroscopy (FCS) has revealed additional information on the fast flickering of GFP variants. A light-driven as well as light-reversed flickering leads to generation of nonfluorescent states of YFP and Citrine with a quantum yield of $\approx 10^{-3}$ (*12, 15*). The microsecond to millisecond time scales of these single-molecule observations may result from strong illumination intensities compared to the low illumination intensity (about 3 orders of magnitude weaker) needed for reversible photobleaching in our bulk experiments. One should also note that the excitation intensity-dependent fast flickering was observed at 488 nm excitation, which preferentially acts on the deprotonated form, and was excitation-dependent, but independent of the pH. Since reversibly photobleached enhanced fluorescent proteins spontaneously recover in the dark (but on a time scale that is not accessible for FCS), the reversible photobleaching in bulk experiments not only appears as reduced quantum efficiency but also results in a variable steady-state equilibrium of fluorescence intensities.

*Implications and Applications for Fluorescence Imaging.* We have demonstrated that, during a typical fluorescence imaging experiment, the fluorescence intensity of a number of enhanced GFP variants reflects a pH- and excitation-dependent variable steady-state equilibrium between reversible photobleaching and spontaneous as well as light-induced recovery. In the past, this effect may have been obscured by the fast adoption of the equilibrium or, in the case of yellow variants, by the distinct wavelength-dependence of reversible photobleaching compared to fluorescence excitation. The quantum efficiencies for reversible photobleaching are more than 100 times greater than those for irreversible photobleaching (*6*). Thus, depending on the actual fraction of protonated species and on the applied wavelength, reversible photobleaching may occur at a rate more than 100-fold greater than the rate of irreversible photobleaching. Therefore, in the design of quantitative multicolor imaging experiments, image acquisition frequencies and illumination intensities should not be changed during the experiment to avoid artifacts due to disturbance of this equilibrium. Moreover, in FRAP or acceptor photobleaching FRET experiments relying on irreversible photobleaching of yellow GFP variants, long wavelengths which neither induce significant reversible photobleaching nor cause light-induced recovery of the donor (e.g. ≥510 nm) should be used. Since the determination of FRAP with eCFP is disturbed by reversible photobleaching, this variant should be either avoided in FRAP experiments or controlled for reversible photobleaching effects. Furthermore, we have shown that the donor photobleaching lifetime is not suitable for assaying

FRET between eCFP and yellow fluorescent proteins, because any wavelength which may be used to bleach eCFP leads to significant reversible or FRET-sensitized irreversible photobleaching of the acceptor. In addition, we have demonstrated that it is possible to assess FRET efficiencies by reversible photobleaching of an acceptor Citrine (see Figure 7). This effect of reversible photochromism may be useful for a repetitive quantitative determination of FRET efficiencies as previously suggested for synthetic fluorochromes (*33*).

## ACKNOWLEDGMENT

We are grateful to Nadine Albrecht for expert technical assistance, and would like to acknowledge the critical discussion with Günter Schultz and H. Peter Reusch. Roger Y. Tsien, San Diego, has kindly provided the cDNA of Citrine.

## REFERENCES

1. Tsien, R. Y. (1998) The green fluorescent protein, *Annu. Rev. Biochem. 67*, 509−544.
2. Miyawaki, A., and Tsien, R. Y. (2000) Monitoring protein conformations and interactions by fluorescence resonance energy transfer between mutants of green fluorescent protein, *Methods Enzymol. 327*, 472−500.
3. Cubitt, A. B., Heim, R., Adams, S. R., Boyd, A. E., Gross, L. A., and Tsien, R. Y. (1995) Understanding, improving and using green fluorescent proteins, *Trends Biochem. Sci. 20*, 448−455.
4. van Thor, J. J., Gensch, T., Hellingwerf, K. J., and Johnson, L. N. (2002) Phototransformation of green fluorescent protein with UV and visible light leads to decarboxylation of glutamate 222, *Nat. Struct. Biol. 9*, 37−41.
5. Heim, R., Cubitt, A. B., and Tsien, R. Y. (1995) Improved green fluorescence, *Nature 373*, 663−664.
6. Griesbeck, O., Baird, G. S., Campbell, R. E., Zacharias, D. A., and Tsien, R. Y. (2001) Reducing the environmental sensitivity of yellow fluorescent protein, *J. Biol. Chem. 276*, 29188−29194.
7. Dickson, R. M., Cubitt, A. B., Tsien, R. Y., and Moerner, W. E. (1997) On/off blinking and switching behaviour of single molecules of green fluorescent protein, *Nature 388*, 355−358.
8. Peterman, E. J. G., Brasselet, S., and Moerner, W. E. (1999) The fluorescence dynamics of single molecules of green fluorescent protein, *J. Phys. Chem. A 103*, 10553−10560.
9. Garcia-Parajo, M. F., Segers-Nolten, G. M. J., Veerman, J. A., Greve, J., and van Hulst, N. F. (2000) Real-time light-driven dynamics of the fluorescence emission in single green fluorescent protein molecules, *Proc. Natl. Acad. Sci. U.S.A.* 97, 7237−7242.
10. Creemers, T. M., Lock, A. J., Subramaniam, V., Jovin, T. M., and Völker. S. (1999) Three photoconvertible forms of green fluorescent protein identified by spectral hole-burning, *Nat. Struct. Biol. 6*, 557−560.
11. Creemers, T. M., Lock, A. J., Subramaniam, V., Jovin, T. M., and Völker, S. (2000) Photophysics and optical switching in green fluorescent protein mutants, *Proc. Natl. Acad. Sci. U.S.A.* 97, 2974−2978.
12. Schwille, P., Kummer, S., Heikal, A. A., Moerner, W. E., and Webb, W. W. (2000) Fluorescence correlation spectroscopy reveals fast optical excitation-driven intramolecular dynamics of yellow fluorescent proteins, *Proc. Natl. Acad. Sci. U.S.A.* 97, 151−156.
13. Schaefer, M., Albrecht, N., Hofmann, T., Gudermann, T., and Schultz, G. (2001) Diffusion-limited translocation mechanism of protein kinase C isotypes, *FASEB J. 15*, 1634−1636.
14. Visser, N. V., Hink, M. A., Borst, J. W., van der Krogt, G. N. M., and Visser, A. J. W. G. (2002) Circular dichroism spectroscopy of fluorescent proteins, *FEBS Lett. 521*, 31−35.
15. Heikal, A. A., Hess, S. T., Baird, G. S., Tsien, R. Y., and Webb, W. W. (2000) Molecular spectroscopy and dynamics of intrinsically fluorescent proteins: Coral red (dsRed) and yellow (Citrine), *Proc. Natl. Acad. Sci. U.S.A.* 97, 11996−12001.
16. Adams, S. R., Kao, J. P. Y., Grynkiewicz, G., Minta, A., and Tsien, R. Y. (1988) Biologically useful chelators that release $Ca^{2+}$ upon illumination, *J. Am. Chem. Soc. 110*, 3212−3220.
17. Hellwig, N., Plant, T. D., Janson, W., Schäfer, M., Schultz, G., and Schaefer, M. (2004) TRPV1 acts as a proton channel to induce acidification in nociceptive neurons, *J. Biol. Chem. 279*, 34553−34561.
18. Miyawaki, A. (2003) Visualization of the spatial and temporal dynamics of intracellular signaling, *Dev. Cell 4*, 295−305.
19. Young, R. M., Arnette, J. K., Roess, D. A., and Barisas, B. G. (1994) Quantitation of fluorescence energy transfer between cell surface proteins via fluorescence donor photobleaching kinetics, *Biophys J. 67*, 881−888.
20. Gadella, T. W. Jr, and Jovin, T. M. (1995) Oligomerization of epidermal growth factor receptors on A431 cells studied by time-resolved fluorescence imaging microscopy. A stereochemical model for tyrosine kinase receptor activation, *J. Cell Biol. 129*, 1543−1558.
21. Damjanovich, S., Vereb, G., Schaper, A., Jenei, A., Matkó, J., Starink, J. P., Fox, G. Q., Arndt-Jovin, D. J., and Jovin, T. M. (1995) Structural hierarchy in the clustering of HLA class I molecules in the plasma membrane of human lymphoblastoid cells, *Proc. Natl. Acad. Sci. U.S.A.* 92, 1122−1126.
22. Patel, R. C., Lange, D. C., Patel, Y. C. (2002) Photobleaching fluorescence resonance energy transfer reveals ligand-induced oligomer formation of human somatostatin receptor subtypes, *Methods 27*, 340−348.
23. Schmid, J. A., Scholze, P., Kudlacek, O., Freissmuth, M., Singer, E. A., and Sitte, H. H. (2001) Oligomerization of the human serotonin transporter and of the rat GABA transporter 1 visualized by fluorescence resonance energy transfer microscopy in living cells, *J. Biol. Chem. 267*, 3805−3810.
24. Scholze, P., Freissmuth, M., and Sitte, H. H. (2002) Mutations within an intramembrane leucine heptad repeat disrupt oligomer formation of the rat GABA transporter 1, *J. Biol. Chem. 46*, 43682−43690.
25. Mekler, V. M., Averbakh, A. Z., Sudarikov, A. B., and Kharitonova, O. V. (1997) Fluorescence energy transfer-sensitized photobleaching of a fluorescent label as a tool to study donor-acceptor distance distributions and dynamics in protein assemblies: studies of a complex of biotinylated IgM with streptavidin and aggregates of concanavalin A, *J. Photochem. Photobiol. B 40*, 278−287.
26. Schaefer, M., Plant, T. D., Stresow, N., Albrecht, N., and Schultz, G. (2002) Functional differences between TRPC4 splice variants, *J. Biol. Chem. 277*, 3752−3759.
27. Haupts, U., Maiti, S., Schwille, P., and Webb, W. W. (1998) Dynamics of fluorescence fluctuations in green fluorescent protein observed by fluorescence correlation spectroscopy, *Proc. Natl. Acad. Sci. U.S.A. 95*, 13573−13578.
28. Hyun Bae, J, Rubini, M., Jung, G., Wiegand, G., Seifert, M. H. J., Azim, M. K., Kim, J.-S, Zumbusch, A., Holak, T. A., Moroder, L., Huber, R., and Budisa, N. (2003) Expansion of the genetic code enables design of a novel "gold" class of green fluorescent proteins, *J. Mol. Biol. 328*, 1071−1081.
29. Elowitz, M. B., Surette, M. G., Wolf, P.-E., Stock, J., and Leibler, S. (1997) Photoactivation turns green fluorescent protein red, *Curr. Biol. 7*, 809−812.
30. Yokoe, H., and Meyer, T. (1996) Spatial dynamics of GFP-tagged proteins investigated by local fluorescence enhancement, *Nat. Biotechnol. 14*, 1252−1256.
31. Patterson, G. H., and Lippincott-Schwartz, J. (2002) A photoactivatable GFP for selective photolabeling of proteins and cells, *Science 297*, 1873−1877.
32. Moerner, W. E., Peterman, E. J. G., Brasselet, S., Kummer, S., and Dickson, R. M. (1999) Optical methods for exploring dynamics of single copies of green fluorescent protein, *Cytometry 36*, 232−238.
33. Song, L., Jares-Erijman, E. A., and Jovin, T. M. (2002) A photochromic acceptor as a reversible light-driven switch in fluorescence resonance energy transfer, *J. Photochem. Photobiol. A 150*, 177−185.

BI047881X